Electronic band structure of magnetic bilayer graphene superlattices

C. Huy Pham, T. Thuong Nguyen, and V. Lien Nguyen

Citation: Journal of Applied Physics **116**, 123707 (2014); doi: 10.1063/1.4896530
View online: http://dx.doi.org/10.1063/1.4896530
View Table of Contents: http://scitation.aip.org/content/aip/journal/jap/116/12?ver=pdfcov
Published by the AIP Publishing

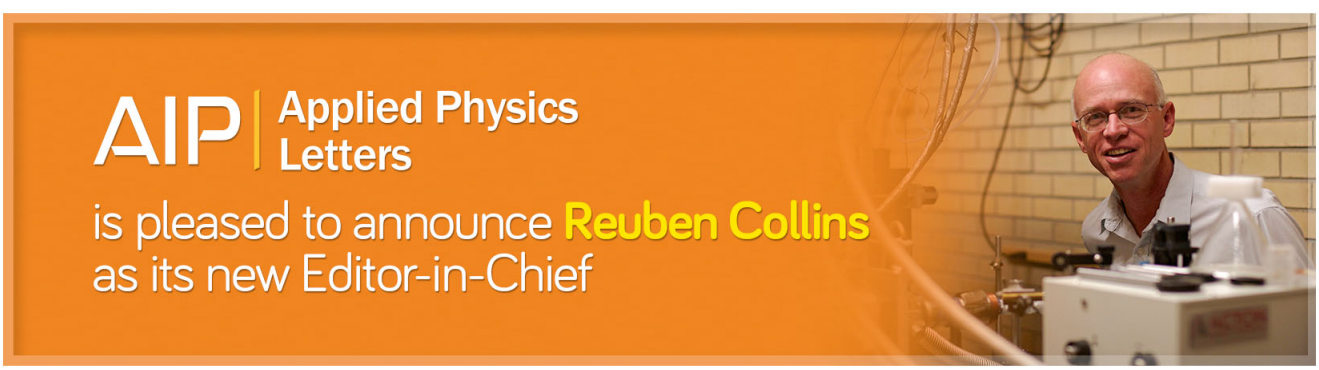

Electronic band structure of magnetic bilayer graphene superlattices

C. Huy Pham,[1,2] T. Thuong Nguyen,[1,2] and V. Lien Nguyen[1,3,a)]
[1]*Theoretical and Computational Physics Department, Institute of Physics, VAST, 10 Dao Tan, Ba Dinh Distr., Hanoi 10000, Vietnam*
[2]*SISSA/International School for Advanced Study, Via Bonomea 265, I-34136 Trieste, Italy*
[3]*Institute for Bio-Medical Physics, 109A Pasteur, 1st Distr., Hochiminh City, Vietnam*

(Received 18 July 2014; accepted 15 September 2014; published online 25 September 2014)

Electronic band structure of the bilayer graphene superlattices with δ-function magnetic barriers and zero average magnetic flux is studied within the four-band continuum model, using the transfer matrix method. The periodic magnetic potential effects on the zero-energy touching point between the lowest conduction and the highest valence minibands of pristine bilayer graphene are exactly analyzed. Magnetic potential is shown also to generate the finite-energy touching points between higher minibands at the edges of Brillouin zone. The positions of these points and the related dispersions are determined in the case of symmetric potentials. © *2014 AIP Publishing LLC*.
[http://dx.doi.org/10.1063/1.4896530]

I. INTRODUCTION

As is well-known from semiconductor physics, the electronic band structure of materials could be essentially modified by an external periodic potential, resulting in unusual transport and optical properties.[1] That is why the electronic band structure of graphene under a periodic potential (graphene superlattice) was extensively studied from the early days of graphene physics. For single layer graphene superlattices (SLGSLs), the electronic band structure has been in detail examined in a number of works for periodic potentials of different natures (electric[2–5] or magnetic[6–10]) and different shapes (Kronig-Penney,[2,5,7,10] cosine,[3] or square[4]). Interesting findings have been reported such as a strongly anisotropic renormalization of the carrier group velocity and an emergence of extra Dirac points (DPs) in the electronic band structure of electric SLGSLs (Refs. 2–5) or an emergence of finite-energy DPs in the electronic band structure of magnetic ones.[8–10]

Concerning the electronic band structure of bilayer graphene superlattices (BLGSLs), there are fewer works and they are all devoted to the case of electric potentials.[11–14] The most impressive feature observed in the electronic band structure of the electric BLGSLs studied (with different potential shapes: δ-function,[11,14] rectangular,[12] or sine[13]) is an emergence of a pair of new zero-energy touching points (TPs) or an opening of a direct band gap, depending on the potential parameters.[15] This unusual feature was not found in the electronic band structure of SLGSLs. It is also assumed to be common for all electric BLGSLs with any potential shape, providing the average potential to be zero.

To our best knowledge, no works on the electronic band structure of BLGSLs with magnetic potentials have been reported. Note that while sharing with single layer graphene many properties important for electronics applications such as the excellent electric and thermal conductivities at room temperature or a possibility to control the electronic structure externally, bilayer graphene (BLG) exhibits the privileges, including the ability to open a band gap in the energy spectrum and to turn it flexibly by an external electric field.[16–18] Given the importance of BLG, it would be appropriate to study the electronic properties of various BLG-based structures.

Graphene superlattices are of not only theoretical but also experimental and application interests. Experimentally, SLGSLs have been constructed for graphene on ruthenium[19] or iridium[20] surfaces. Other possible techniques that may be applied for creating SLGSLs as well as BLGSLs include the electron-beam induced deposition of adsorbates[21] and the use of periodically patterned gates. The very fact that the band structure of graphene superlattices may be finely engineered by using appropriate periodic potentials opens different ways to fabricate graphene-based electronic devices.

The purpose of the present work is to study the electronic band structure of BLGSLs with periodic δ-function magnetic barriers (magnetic BLGSLs—MBLGSLs). It is shown that the studied magnetic potential does not destroy the isotropically parabolic behavior of the band dispersion related to the original zero-energy TP, but makes the corresponding effective mass renormalized and might cause a shift of this point along the direction perpendicular to the superlattice direction in the wave-vector space. The magnetic potential is also shown to generate finite-energy TPs with linear and anisotropic dispersions at the edges of Brillouin zone. These findings make the band structure of MBLGSLs cardinally different from that of electric BLGSLs examined.

The paper is organized as follows. Section II describes the model of MBLGSLs under study and the calculating method. Section III presents calculating results which are in detail analyzed with an attention focused on the TPs identified at zero- as well as finite-energies. The paper is closed with an additional discussion and a brief summary in Sec. IV.

II. MODEL AND CALCULATING METHOD

We consider MBLGSLs arising from an infinitely flat Bernal-stacked BLG in a periodic magnetic field illustrated

a)Electronic mail: nvlien@iop.vast.ac.vn

schematically in Fig. 1(a). The magnetic field is assumed to be uniform in the y-direction and staggered as periodic δ-function barriers of alternate signs in the x-direction, so for a single lattice unit the field profile has the form

$$\vec{B} = B_0[\delta(x + d_B/2) - \delta(x - d_B/2)]\hat{z}, \tag{1}$$

where B_0 is the barrier strength and d_B is the barrier width. The corresponding vector potential $\vec{A}$ in the Landau gauge is

$$\vec{A}(x) = (B_0 l_B/2)\,[\theta(d_B/2 - |x|) - \theta(|x| - d_B/2)]\hat{y}, \tag{2}$$

where $\theta(x)$ is the Heaviside step function and $l_B = \sqrt{\hbar c/eB_0}$ is the magnetic length.

Totally, as can be seen in Fig. 1(b), $A(x)$ describes a Kronig-Penney-type periodic potential along the x-direction with d_B is the barrier width, d_W is the well width, $d = d_B + d_W$ is the superlattice period, and $A_0 \equiv B_0 l_B$ is the potential strength.

In fact, the same periodic δ-function magnetic barriers of Eq. (1) have been before used to model magnetic SLGSLs.[6,7,10] Its advantage is a richness of fundamental electronic properties, while a mathematical treatment is rather simple. In practice, such the δ-function model should be hold as long as the de Broglie wavelength of quasiparticles is much larger than the typical width of magnetic barriers.[6]

To justify the consideration realized below, we will ignore intervalley scattering assuming that the widths $d_{B(W)}$ are much larger than the lattice constant in graphene. All spin-related effects are also neglected. Besides, potentials on both graphene layers are assumed to be the same at a given (x, y)-point. Under these conditions, the low-energy excitations near one original TP (say, K) in the energy band structure can be generally described in the four-band continuum nearest-neighbor, tight-binding model with the Hamiltonian[22]

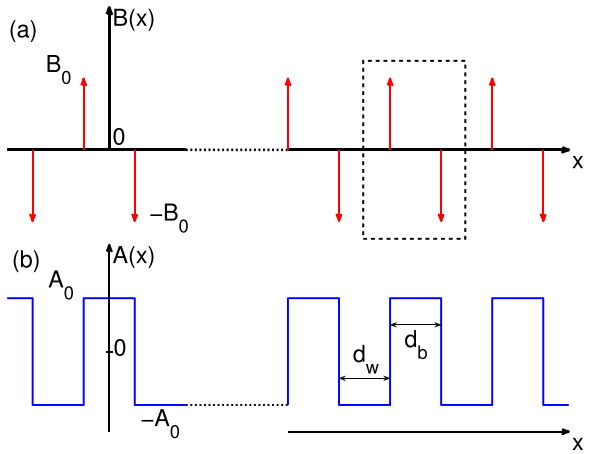

FIG. 1. Model of MBLGSLs under study: (a) Periodic δ-function magnetic barriers of alternate signs, $\vec{B}_0$ and $-\vec{B}_0$ [red arrows] and (b) corresponding 1D periodic vector potential $\vec{A}(x)$ [blue curve] with A_0 the potential strength, d_B is the barrier width, and d_W is the well width [the period $d = d_B + d_W$]. The dashed-line box in (a) describes the unit cell in T-matrix calculations.

$$H = \begin{pmatrix} 0 & v_F\hat{\pi} & t_\perp & 0 \\ v_F\hat{\pi}^+ & 0 & 0 & 0 \\ t_\perp & 0 & 0 & v_F\hat{\pi}^+ \\ 0 & 0 & v_F\hat{\pi} & 0 \end{pmatrix}, \tag{3}$$

where $\hat{\pi} = p_x + ip_y$, $v_F = \sqrt{3}\mathrm{ta}/(2\hbar) \approx 10^6\,\mathrm{m/s}$ is the Fermi velocity, $t \approx 3\,\mathrm{eV}$ is the intralayer nearest-neighbor hopping energy, $a = 2.46\,\text{Å}$ is the lattice constant of graphene, and $t_\perp \approx 0.39\,\mathrm{eV}$ is the interlayer nearest-neighbor hopping energy. The magnetic field effect is here accounted for by the momentum operator $\vec{p} = (p_x, p_y) \equiv -i\hbar\vec{\nabla} + e\vec{A}$. The Hamiltonian of Eq. (3) is limited to the case of symmetric on-site energies. Also, other interlayer hopping parameters are here neglected since they are much smaller than $t_\perp$ and may be effectively suppressed by disorder.[17,18,23]

Without the potential $\vec{A}$, i.e., for pristine BLG, the Hamiltonian of Eq. (3) yields the hyperbolic band dispersion which interpolates between a linear dispersion at large momentum and a quadratic one in the vicinity of the TP.[18] Such a hyperbolic BLG band dispersion was experimentally observed[24,25] and, interestingly, it is still survived (with renormalized parameters) even if the electron-electron interaction is taken into account.[23,26] We are here interested in the effects induced by the periodic magnetic potential $\vec{A}$ on the BLG non-interacting band structure.

Due to a periodicity of the potential A (along the x-direction) the time-independent Schrödinger equation $H\Psi = E\Psi$ for the Hamiltonian H of Eq. (3) could be most conveniently solved using the transfer matrix method.[11,27] Actually, our ultimate aim is to find the $E(\vec{k})$-relation that describes the band structure of MBLGSLs under study. This could be done in the way similar to that realized in Ref. 11 for electric BLGSLs in the four band model.

Following the general idea of the T-matrix method,[27] we first consider the wave functions of the equation $H\Psi = E\Psi$ in the regions of constant potential, $A(x) = A_0 = constant$. For H of Eq. (3) these wave functions can be generally written in the form $\Psi = QR(x)[A, B, C, D]^T \exp(ik_y y)$. They can be then simplified by the linear transformation $Q \to \mathcal{T}Q$ with[11]

$$\mathcal{T} = \frac{1}{2}\begin{pmatrix} 1 & 0 & -1 & 0 \\ 0 & 1 & 0 & -1 \\ 1 & 0 & 1 & 0 \\ 0 & 1 & 0 & 1 \end{pmatrix}.$$

So

$$Q \to \mathcal{T}Q = \begin{pmatrix} 1 & 1 & 0 & 0 \\ k_1/E & -k_1/E & -ik'_y/E & -ik'_y/E \\ 0 & 0 & 1 & 1 \\ -ik'_y/E & -ik'_y/E & k_2/E & -k_2/E \end{pmatrix}, \tag{4}$$

whereas the $\mathcal{T}$-transformation does not change the matrix $R(x)$

$$R(x) = diag\,[e^{ik_1 x}, e^{-ik_1 x}, e^{ik_2 x}, e^{-ik_2 x}], \tag{5}$$

where $k'_y = k_y + A_0$ and $k_n = \sqrt{E^2 - (-1)^n E - k_y^2}$ with $n = 1, 2$.

Further, the amplitudes $\mathcal{A}_I$ of the wave function before an unit cell and those after it, $\mathcal{A}_F$, could be related to each other by the T-matrix

$$\mathcal{A}_F = T(F, I)\mathcal{A}_I. \tag{6}$$

On the other hand, the Bloch's theorem states

$$Q_I R_I(x)\mathcal{A}_F = \exp(ik_x d) Q_I R_I(x - d)\mathcal{A}_I, \tag{7}$$

where k_x is the Bloch wave number and d is the potential period.

Comparing Eq. (6) with Eq. (7) gives rise to the following equation:

$$det\,[T - e^{ik_x d} R_I^{-1}(d)] = 0. \tag{8}$$

This is just the equation solutions of which give the desirable $E(\vec{k})$-relation.

In reality, the transfer matrix Eq. (8) is very general with matrices $T \equiv T(F, I)$ and R_I defined by the Hamiltonian examined. For the Hamiltonian under study, with the unit cell described in Fig. 1(a), the T-matrix in Eq. (8) is defined as

$$T(F, I) = R_W^{-1}(d_B) Q_W^{-1} Q_B R_B(d_B) Q_B^{-1} Q_W\,,$$

where $Q_{W(B)}$ and $R_{W(B)}$ are, respectively, defined in Eqs. (4) and (5) for $A_0 = A_{W(B)}$ and $R_I \equiv R_W$.

In the case of SLGSLs, when the Hamiltonian H and, therefore, T and R_I are 2×2 matrices, Eq. (8) can be analytically solved that gives straightaway a general expression for the dispersion relation, $E(\vec{k})$.[10] For MBLGSLs in the four-band model of Eq. (3), Eq. (8) with (4×4)-matrices T and R_I becomes too complicated. It cannot be in general solved analytically and, therefore, the dispersion relation cannot be derived explicitly.

Note that for the periodic magnetic potential model of interest the only way of breaking its symmetry is associated with a difference between d_B and d_W. So the parameter $q = d_W/d_B$ is introduced to describe asymmetric effects. The MBLGSLs with $q = 1$ ($q \neq 1$) will be then referred to as symmetric (asymmetric) MBLGSLs. Thus, the studied potential model is entirely characterized by the three parameters, A_0, d, and q.

III. ELECTRONIC BAND STRUCTURES

In order to bring out the band structure of a MBLGSL, we should numerically solve Eq. (8) for defined values of parameters A_0, d, and q. Calculations have been performed for different values of these parameters and typical results obtained are presented in Figs. 2 and 3.

Zero-energy TP—Figs. 2(a), 2(c), and 2(e) show the lowest conduction and the highest valence minibands in the energy spectra of the MBLGSLs with $A_0 = 0.5$, $d = 4$, and different values of q: (a) $q = 1$ (symmetric MBLGSLs), (c) $q = 1.5$, and (e) $q = 0.5$ (asymmetric MBLGSLs). The boxes (b), (d), and (f) present the contour plots of the lowest

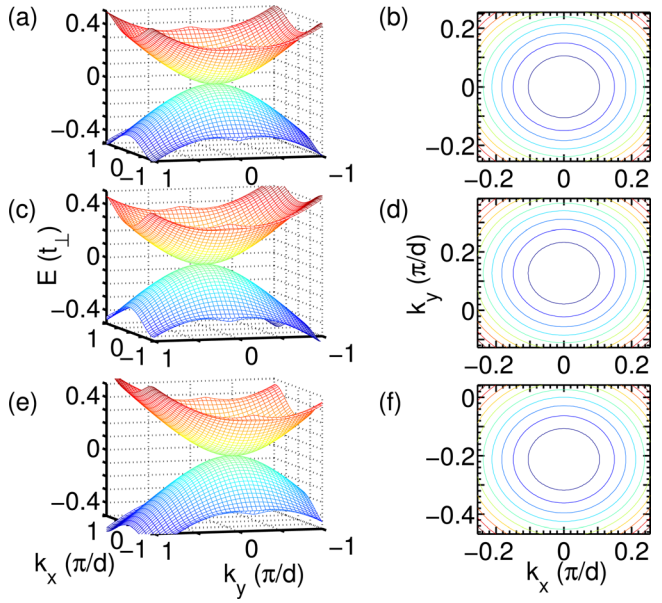

FIG. 2. Zero-energy TP. Lowest conduction and highest valence minibands [(a), (c), and (e)] and corresponding contour plots [(b) to (a), (d) to (c), and (f) to (e)] are shown in three cases: $q = 1$ [(a) and (b)], $q = 1.5$ [(c) and (d)], and $q = 0.5$ [(e) and (f)]. In all the cases: $d = 4$ and $A_0 = 0.5$. The zero-energy TP is found at $(E, k_x, k_y) = (0, 0, 0)$ in ((a), (b)); $(0, 0, 0.1)$ in ((c), (d)); and $(0, 0, -0.167)$ in ((e), (f)). All contour plots show isotropic dispersions.

conduction miniband for the energy spectra shown in (a), (c), and (e), respectively. (Due to a symmetry of spectra with respect to the $(E = 0)$-plane, the analysis is hereafter concentrated on the positive energy part). For comparison, we recall that in the band structure of the pristine BLG there is a single zero-energy TP located at $\vec{k} = 0$ (i.e., the K-point), in the vicinity of which the dispersion has the parabolic shape: $E = \pm\hbar^2 k^2/2m$ with the isotropic mass $m = t_\perp/2v_F^2$.[18] Below, for convenience, dimensionless quantities are introduced: A_0 in

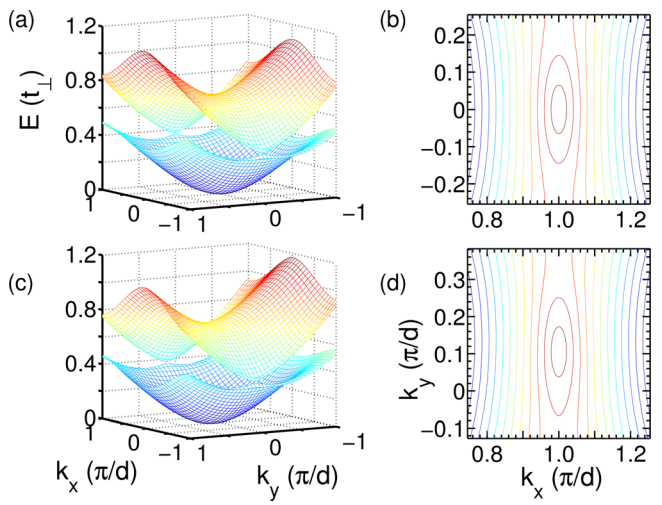

FIG. 3. Finite-energy TP. Two lowest conduction minibands [(a) and (c)] and corresponding contour plots [(b) to (a) and (d) to (c)] are shown in two cases: $q = 1$ [(a) and (b)] and $q = 1.5$ [(c) and (d)]. In both cases: $d = 4$ and $A_0 = 0.5$. Clearly, there is a TP at the edge of Brillouin zone, $k_x = \pi/d$ [or, in equivalence, $k_x = -\pi/d$], which is located at $(E, k_x, k_y) = (E_1 \approx 0.37\, t_\perp, 0, 0)$ in (a) or $(E_1 \approx 0.375\, t_\perp, 0, k_y^{(f)} \approx 0.09)$ in (c). Contour plots in (b) and (d) show anisotropic dispersions.

units of $t_\perp/(ev_F)$, energies in units of $t_\perp$, and x (or d) in $(\hbar v_F/t_\perp)$. For example, the value $A_0 = 0.5$ describes the field of $B_0 = 2.3$ T or $d = 4$ means the period of 6.75 nm, given $t_\perp$ and v_F as defined above.

In the case of $q = 1$ (symmetric MBLGSLs), Fig. 2(a) shows a clear zero-energy TP between the two minibands at $(\vec{k} = 0)$ with an isotropic band dispersion [see contour plot in (*b*)]. It seems that in this particular case of $k_y = 0$, the matrices in Eq. (8) become so simple that the energy spectrum can be from this equation deduced in the form of the transcendental equation

$$\begin{aligned}&[\cos(k_x d) - \cos(k_1 d)][\cos(k_x d) - \cos(k_2 d)]\\&+(4A_0^4/k_1^2k_2^2)\sin(k_1 d_W)\sin(k_1 d_B)\sin(k_2 d_W)\sin(k_2 d_B)\\&+(2A_0^2/k_1 k_2)[f_1 + f_2\cos(k_x d) - \sin(k_1 d)\sin(k_2 d)] = 0,\end{aligned} \tag{9}$$

where $f_1 = \sin(k_1 d_W)\sin(k_2 d_W) + \sin(k_1 d_B)\sin(k_2 d_B), f_2 = \sin(k_1 d_W)\sin(k_2 d_B) + \sin(k_1 d_B)\sin(k_2 d_W)$, and $k_{1(2)} = \sqrt{E^2 \pm E - A_0^2}$.

Next, expanding Eq. (8) to the lowest order in E, k_x, and k_y we straightaway obtain the band dispersion in the vicinity of the zero-energy TP examined

$$E = \pm\hbar^2 k^2/2m^* \text{ with } m^* = m\frac{A_0 d}{2\sinh(A_0 d/2)}. \tag{10}$$

This dispersion has the same isotropically parabolic shape as that for the pristine BLG, but the effective mass is renormalized, depending on the product $(A_0 d)$ as a single parameter.

Thus, impressively, the only effect a symmetrically periodic magnetic potential $[q = 1]$ can cause on the original zero-energy TP is making the effective mass renormalized. Equation (10) shows that m^* is always less than m (for the pristine BLG): $(m^*/m) \to 1$ at $A_0 d \ll 1$ and $\to 0$ in the limit of large $A_0 d$.

Now, we consider the more general case of asymmetric MBLGSLs $[q \neq 1]$. In this case, as can be seen in Fig. 2, the most noticeable feature is the magnetic potential induced shift of the original zero-energy TP along the $(k_x = 0)$-direction in either the positive [if $q > 1$, see Figs. 2(c) and 2(d)] or the negative direction of k_y [if $q < 1$, see Figs. 2(e) and 2(f)]. An intuitive estimation reveals that the magnetic potential shifts the zero-energy TP from the original $(E = 0, k_x = 0, k_y = 0)$-point to the $(E = 0, k_x = 0, k_y = k_y^{(q)})$-point with $k_y^{(q)}$ depending on the potential parameters as $k_y^{(q)} = [(q-1)/(q+1)]A_0$. In Figs. 2(c) and 2(d) $[q = 1.5]$ or 2(e) and 2(f) $[q = 0.5]$, the $k_y^{(q)}$-coordinate is equal to 0.1 or ≈ -0.167, respectively (given $A_0 = 0.5$). Note that $k_y^{(q)}$ does not depend on the superlattice period d.

Further, as can be seen in Figs. 2(d) and 2(f), it seems that even for asymmetric MBLGSLs, the band dispersion in the vicinity of the zero-energy TP is still isotropic. This statement could be justified in the way introduced in Refs. 5 and 14, writing Eq. (8) in the form $f(E, k_x, k_y) = 0$, then expanding f to the lowest order in E, k_x, and k_y in the vicinity of the TP examined, i.e., the $(E = 0, k_x = 0, k_y = k_y^{(q)})$-point. In the result, we obtain the relation

$$E = \pm\frac{\hbar^2}{2m_q^*}[k_x^2 + (k_y - k_y^{(q)})^2] \tag{11}$$

with the mass m_q^* depending on A_0, d, and q as

$$m_q^* = m\frac{2qA_0 d}{(q+1)^2\sinh(2qA_0 d/(q+1)^2)}. \tag{12}$$

These equations show that while moving the zero-energy TP along the k_y-direction from $k_y = 0$ to $k_y = k_y^{(q)}$, the asymmetrically periodic magnetic potentials keep the related band dispersion isotropically parabolic and electron-hole symmetric with an effective mass renormalized, depending on $(A_0 d)$ and q. Certainly, Eqs. (11) and (12) are reduced to Eq. (10) in the case of $q = 1$.

Like m^* in Eq. (10), the mass m_q^* in Eq. (12) is always less than m (for the pristine BLG) and the ratio m_q^*/m monotonously decreases with increasing the product $(A_0 d)$. Given $(A_0 d)$, the mass m_q^* varies with q, reaching a single minimum at $q = 1$ (i.e., for symmetric potentials), where $m_q^* = mA_0 d/2\sinh(A_0 d/2)$.

Thus, a shift in k_y-coordinate and a renormalization of effective mass are the only two effects the periodic magnetic potential studied can induce on the zero-energy TP in the energy band structure of BLG.

Finite-energy TPs—Fig. 3 shows the two lowest conduction minibands [(a) and (c)] and the corresponding contour plots [(b) to (a) and (d) to (c)] for just the two MBLGSLs examined in Figs. 2((a) and (b)) and 2((c) and (d)). In both the cases, $q = 1$ ((a) and (b)) and $q = 1.5$ ((c) and (d)), it is clear that (*i*) there exist the finite energy TPs between the two minibands at the edges of the Brillouin zone, $(k_x = \pm\pi/d, k_y = k_y^{(f)})$, where $k_y^{(f)}$ depends on A_0 and q and equals to zero in the case of $q = 1$ (symmetric MBLGSLs) [Figs. 3(a) and 3(b)] and (*ii*) the band dispersions related to these TPs are anisotropic [Figs. 3(b) and 3(d)]. Similar TPs between minibands are also existed at higher energies (not shown). Describing quantitatively these TPs is generally beyond our ability except the case of symmetric MBLGSLs, when $k_y^{(f)} = 0$. In this case, with zero k_y-coordinate, the energy location as well as the band dispersion related to the finite energy TPs observed can be found from Eq. (9) in the same way as that used above for the zero-energy DP.

Indeed, for symmetric MBLGSLs, substituting the coordinates $k_x = \pm\pi/d$ and $k_y = 0$ of the finite-energy TPs into Eq. (9), we obtain the relation

$$\cos(k_1 d/2)\cos(k_2 d/2) - (A_0^2/k_1 k_2)\sin(k_1 d/2)\sin(k_2 d/2) = 0, \tag{13}$$

where $k_{1(2)} = \sqrt{E^2 \pm E - A_0^2}$. This equation yields the energy-coordinates E_n of all finite-energy TPs generated at the edges of the Brillouin zone in the energy spectra of the symmetric MBLGSL, given A_0 and d. So, these TPs are located at $(E = E_n, k_x = \pm\pi/d$, and $k_y = 0)$.

To find $\{E_n\}$, we numerically solved Eq. (13) for different values of A_0 and d. Some results obtained are presented,

for example, in Fig. 4, where the three lowest energies E_n ($n=1$, 2, 3) are plotted as a function of A_0 [Fig. 4(a) for $d=4$] or d [Fig. 4(b) for $A_0=0.5$]. Fig. 4(a) shows that while the only position E_1 of the lowest finite-energy touching point is slightly descended, the positions of higher touching points [$E_{2,3}$ in the figure and higher E_n not shown] considerably rise with increasing the potential strength A_0. Fig. 4(b) shows that all the energies E_n fall sharply at $d \leq 5$ and then smoothly decrease at larger period d. Particularly, in Fig. 3(a), the lowest finite energy TP is located at $E_1 \approx 0.37\, t_\perp$.

Next, to understand the anisotropic contour plots in Fig. 3(b), we have to find the dispersion relation, following the same way as described above. Thus, by expanding Eq. (8) in the vicinity of the ($E=E_n$, $k_x=\pi/d$, and $k_y=0$)-point, we arrive at the linear dispersion relation

$$E - E_n = \pm\sqrt{v_{nx}^2(k_x-\pi/d)^2 + v_{ny}^2 k_y^2}, \qquad (14)$$

where v_{nx} and v_{ny} are carrier group velocity components depending on A_0 and d. With the dispersions of Eq. (14), the finite-energy TPs studied could be really referred to as the finite-energy DPs.

Unfortunately, we are unable to derive analytical expressions for the velocities v_{nx} and v_{ny}. So, for instance, we show in Fig. 4, the numerical values of v_{1x} [solid line] and v_{1y} [dashed line] plotted against the potential strength A_0 [Fig. 4(c)] or the period d [Fig. 4(d)] for the lowest (and most important) finite-energy DP ($n=1$). At small A_0 and/or d, a large difference between the two velocities, $v_{1x} \gg v_{1y}$, demonstrates a strongly anisotropic dispersion. Given d [Fig. 4(c)] (or A_0 [Fig. 4(d)]), there exists a single value of $A_0 = A_0^{(c)}$ (or $d=d^{(c)}$), where $v_{1x}=v_{1y}$ showing an isotropic dispersion [$A_0^{(c)} \approx 1.5$ in Fig. 4(c) and $d^{(c)} \approx 10.435$ in Fig. 4(d)]. Beyond this point, an anisotropy in dispersion is recovered, but it is much weaker than in the region of small A_0 and/or d. Returning to Figs. 3(a) and 3(b) for the symmetric MBLGSL with $A_0=0.5$ and $d=4$, we have $v_{1x}/v_{1y} \approx 2.1$. This result explains a anisotropy in the contour plots in Fig. 3(b). For higher finite-energy DPs ($n=2$, 3,…), calculations show much more complicated A_0- and d-dependences of velocities (not shown) that demonstrate a strongly anisotropic dispersion at small as well as large values of A_0 and/or d except a single point where $v_{nx}=v_{ny}$.

In the opposite case of asymmetric MBLGSLs, $q \neq 1$ [Figs. 3(c) and 3(d)], we are able only to qualitatively comment that the finite-energy TPs with linear dispersion should be still generated at the edges of the Brillouin zone, $k_x=\pm\pi/d$, but at non-zero $k_y = k_y^{(f)}$ and at energies which depend on potential parameters in the way much more complicated than Eq. (13) [in Figs. 3(c) and 3(d) $k_y^{(f)} \approx 0.09$ and $E_1 \approx 0.375\, t_\perp$].

Density of States—With the band structure determined we can calculate its most important characteristics—the density of states (DOS). Calculations have been performed in the same way as that suggested for SLGSLs in Ref. 7.

Fig. 5(a) shows as an example of the DOS for the MBLGSL studied in Fig. 3(a) [red solid line] in comparison to that for the pristine BLG [blue dashed line]. The arrow indicates the energy-position of the lowest finite energy DP, E_1, calculated in Fig. 4(a). It should be first noted that the step jump at $|E| \to 0$ in both the DOS-curves, solid for MBLGSL as well as dashed for pristine BLG, are associated with the parabolic shape of the band dispersion in the vicinity of the neutral point. At larger $|E|$, clearly, the periodic magnetic potential makes the solid line rather fluctuated, comparing to the dashed one. A similar fluctuation has been observed in the DOSs of SLGSLs[4] and electric BLGSLs.[14] Such a periodic potential induced fluctuation in the DOS should be certainly manifested itself in transport properties of the structure.

To understand the DOS-fluctuation observed, we present in Fig. 5(b) the cut of the band structure along the ($k_y=0$)-plan for the same MBLGSL with DOS shown in Fig. 5(a). The dips at finite energies in the DOS solid curve in Fig. 5(a) are clearly associated with the TPs seen in Fig. 5(b), whereas

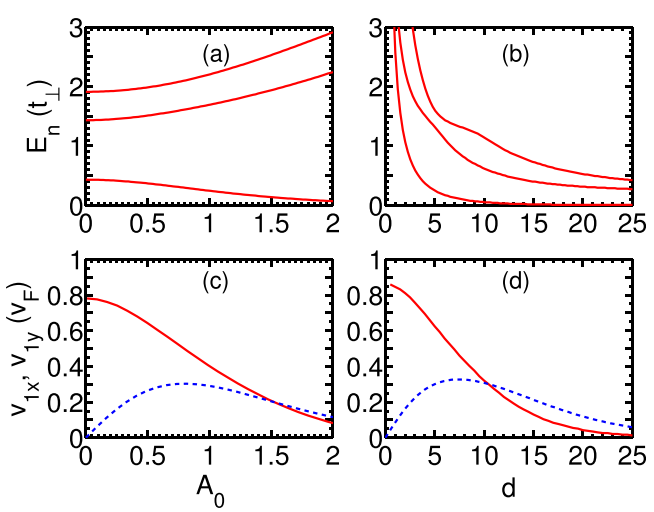

FIG. 4. Three lowest from E_n determined in Eq. (13) are plotted versus A_0 [(a) for $d=4$] or d [(b) for $A_0=0.5$], $n=1$, 2, and 3 (from bottom). In (c) or (d) velocities v_{1x} [red solid line] and v_{1y} [blue dashed line] in Eq. (14) versus A_0 [(c) for $d=4$] or d [(d) for $A_0=0.5$], respectively.

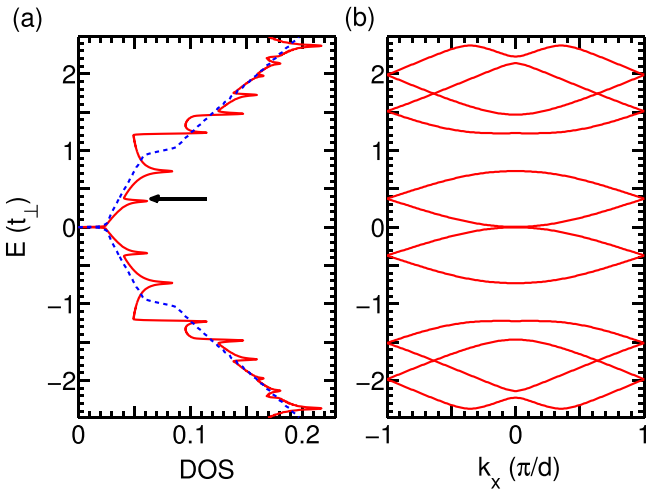

FIG. 5. (a) DOS for the MBLGSL with energy band structure presented in Fig. 3(a) [red solid line] and that for the pristine BLG [blue dashed line] are compared [arrow indicates the energy position E_1 of the lowest finite energy DPs]; (b) Cut along the ($k_y=0$)-plane of the band structure with the DOS shown in (a).

the peaks are located at the bending points between these TPs. Note that Fig. 5(b) also shows the TPs other than those studied above. These TPs are however generated only at higher energies and, therefore, should be less important from transport properties point of view.

IV. CONCLUSION

We have studied the effects of a periodic δ-function magnetic field with zero average flux (say, along the x-direction) on the electronic band structure of BLGs. The potential is characterized by the three parameters: the strength A_0, the period d, and the asymmetric factor q (the ratio between the well width and the barrier width). It was shown that the magnetic potential (*i*) may move the original zero-energy TP between the lowest conduction and the highest valence minibands along the k_y-direction from $k_y = 0$ to a k_y-coordinate, which depends on q and A_0 and equals to zero for symmetric potentials with $q = 1$; (*ii*) does not destroy the isotropically parabolic shape of the band dispersion related to this TP, but makes the effective mass renormalized, depending on the potential parameters; and (*iii*) generates the finite-energy TPs between minibands at the edges of the Brillouin zone, the position of which and the related anisotropically linear dispersion are exactly identified in the case of symmetric potentials. These finite-energy DPs manifest themselves in the fluctuation behavior of the density of states and, therefore, should cause some effect on the transport properties of MBLGSLs.

For comparison, remind two related systems: electric BLGSLs considered in Refs. 11–14 and magnetic SLGSLs considered in Refs. 6, 7, and 10 for the potential with the same shape of Eqs. (1) and (2). In the former systems, the electric potential replaces the original zero-energy TP with either a pair of new zero-energy TPs or a direct band gap, depending on the potential parameters.[11–14] It may also generate the finite-energy TPs with direction-dependent dispersions.[14] In the latter, the magnetic potential leads to the effects rather similar to those found in the present work, including a potential induced shift of the zero-energy TP, an isotropic renormalization of the group velocity related to this point, and an emergence of finite energy DPs.[10] We assume that the findings shown above for MBLGSLs with δ-function magnetic barriers should robust against the changes in the shape of magnetic barrier, providing the average flux to be zero.

It should be finally noted that the MBLGSLs with δ-function magnetic barriers studied in the present work may be realized using, for example, the narrow ferromagnetic strips deposited on the top a BLG (see for a review[28]). Recently, much attention is given to the substrate induced graphene superlattices such as the graphene hexagonal boron nitride moiré superlattices (see Refs. 29 and 30 and references therein).

ACKNOWLEDGMENTS

This work was financially supported by Vietnam National Foundation for Science and Technology Development under Grant No. 103.02-2013.17.

[1]L. Esaki and R. Tsu, IBM J. Res. Dev. **14**, 61 (1970).
[2]C.-H. Park, L. Yang, Y.-W. Son, M. L. Cohen, and S. G. Louie, Nat. Phys. **4**, 213 (2008); Phys. Rev. Lett. **101**, 126804 (2008); **103**, 046808 (2009).
[3]L. Brey and H. A Fertig, Phys. Rev. Lett. **103**, 046809 (2009).
[4]M. Barbier, P. Vasilopoulos, and F. M. Peeters, Phys. Rev. B **81**, 075438 (2010).
[5]C. H. Pham, H. C. Nguyen, and V. L. Nguyen, J. Phys.: Condens. Matter **22**, 425501 (2010).
[6]S. Ghosh and M. Sharma, J. Phys.: Condens. Matter **21**, 292204 (2009).
[7]M. R. Masir, P. Vasilopoulos, and F. M. Peeters, J. Phys.: Condens. Matter **22**, 465302 (2010).
[8]I. Snyman, Phys. Rev. B **80**, 054303 (2009).
[9]L. Dell' Anna and A. De Martino, Phys. Rev. B **83**, 155449 (2011).
[10]V. Q. Le, C. H. Pham, and V. L. Nguyen, J. Phys.: Condens. Matter **24**, 345502 (2012).
[11]M. Barbier, P. Vasilopoulos, and F. M. Peeters, Phys. Rev. B **82**, 235408 (2010).
[12]M. Killi, S. Wu, and A. Paramekanti, Phys. Rev. Lett. **107**, 086801 (2011).
[13]L. Z. Tan, C.-H. Park, and S. G. Louie, Nano Lett. **11**, 2596 (2011).
[14]C. H. Pham and V. L. Nguyen, "Touching points in the energy band structure of bilayer graphene superlattices," J. Phys.: Condens. Matter (to be published).
[15]Though these TPs are somewhere called DPs,[12,13] strictly, the band dispersion in the vicinity of a DP should be not only electron-hole symmetric but also linear. The "touching point" terminology used here is more general regardless of the dispersion shape as well as the energy position (zero or finite).[11,14]
[16]E. V. Castro, K. S. Novoselov, S. V. Morozov, N. M. R. Peres, J. M. B. Lopes dos Santos, J. Nilsson, F. Guinea, A. K. Geim, and A. H. Castro Neto, J. Phys.: Condens. Matter **22**, 175503 (2010).
[17]S. Das Sarma, S. Adam, E. H. Hwang, and E. Rossi, Rev. Mod. Phys. **83**, 407 (2011).
[18]E. McCann and M. Koshino, Rep. Prog. Phys. **76**, 056503 (2013).
[19]S. Marchini, S. Günther, and J. Wintterlin, Phys. Rev. B **76**, 075429 (2007).
[20]J. Coraux, A. T. N'Diaye, C. Busse, and T. Michely, Nano Lett. **8**, 565 (2008).
[21]J. C. Meyer, C. O. Girit, M. F. Crommie, and A. Zettl, Appl. Phys. Lett. **92**, 123110 (2008).
[22]It was shown that at least for the δ-function potentials the two-band model is not accurate enough for describing the energy band structure of BLGSLs, so the four-band model should be applied.[11]
[23]S. V. Kusminskiy, D. K. Campbell, and A. H. Castro Neto, Europhys. Lett. **85**, 58005 (2009).
[24]E. A. Henriksen, Z. Jiang, L.-C. Tung, M. E. Schwartz, M. Takita, Y.-J. Wang, P. Kim, and H. L. Stormer, Phys. Rev. Lett. **100**, 087403 (2008).
[25]E. A. Henriksen and J. P. Eisenstein, Phys. Rev. B **82**, 041412(R) (2010).
[26]K. Zou, X. Hong, and J. Zhu, Phys. Rev. B **84**, 085408 (2011).
[27]H. C. Nguyen and V. L. Nguyen, J. Phys.: Condens. Matter **21**, 045305 (2009).
[28]A. Nagoret, J. Phys.: Condens. Matter **22**, 253201 (2010).
[29]M. Mucha-Kruczynski, J. R. Wallbank, and V. I. Fal'ko, Phys. Rev. B **88**, 205418 (2013).
[30]P. Moon and M. Koshino, e-print arXiv:1406.0668.